Meccanica
DOI 10.1007/s11012-013-9828-2

Linear stability of particle laden flows: the influence of added mass, fluid acceleration and Basset history force

Joy Klinkenberg · H.C. de Lange · Luca Brandt

Received: 19 February 2013 / Accepted: 17 October 2013

Abstract Both modal and non-modal linear stability analysis of a channel flow laden with particles is presented. The particles are assumed spherical and solid and their presence modelled using two-way coupling, with Stokes drag, added mass and fluid acceleration as coupling terms. When the particles considered have a density ratio of order one, all three terms become important. To account for the volume and mass of the particles, a modified Reynolds number is defined. Particles lighter than the fluid decrease the critical Reynolds number for modal stability, whereas heavier particles may increase the critical Reynolds number. Most effect is found when the Stokes number defined with the instability time scale is of order one. Non-modal analysis shows that the generation of streamwise streaks is the most dominant disturbance-growth mechanism also in flows laden with particles: the transient growth of the total system is enhanced proportionally to the particle mass fraction, as observed previously in flows laden with heavy particles. When studying the fluid disturbance energy alone, the optimal growth hardly changes. We also show that the Basset history force has a negligible effect on stability. The inclusion of the extra interaction terms does not show any large modifications of the subcritical instabilities in wall-bounded shear flows.

Keywords Linear stability analysis · Modal analysis · Non-modal analysis · Particle-laden flows

1 Introduction

Particle laden flows are found in our environment and engineering applications, e.g. sand in the atmosphere, soot in gas flows and turbines. Indeed, significant efforts have been recently devoted to the study of particles in turbulence as reviewed in Refs. [1] and [2]. Already in the early '60, it has been shown that adding dust to a pipe flow reduces the drag [3]. As an explanation for this phenomenon, it has been proposed that the interaction between fluid and particles damps the initiation and growth of disturbances which then leads to turbulent structures. Turbulent structures enhance drag, thus, if turbulence is delayed, drag can be reduced. Drag reduction in flows with light and heavy particles has been demonstrated experimentally later on in several papers [4–6]. Numerically, it is found that micro-bubbles, which can be modeled as rigid spheres when the bubbles are small enough, reduce drag in a turbulent flow [7, 8]. On the other hand, simulations of drag reduction by means of heavy particles are presented in [9].

J. Klinkenberg (✉) · H.C. de Lange
Technische Universiteit Eindhoven, Postbus 513,
5600 MB, Eindhoven, The Netherlands
e-mail: j.klinkenberg@tue.nl

J. Klinkenberg · L. Brandt
Linné Flow Centre, KTH Mechanics, 100 44, Stockholm,
Sweden

Published online: 06 November 2013

These findings motivate us to investigate whether the laminar-turbulent transition can be delayed using particles, while we studied the case of heavy particles in previous papers [10, 11]. Here we denote by heavy particles those whose density is significantly larger than the fluid density and the interaction between fluid and particles is given by the Stokes Drag only. When lighter particles are considered, instead, Stokes drag alone is not sufficient to describe the fluid-particle interaction. The present study focuses therefore on the effect of the other interaction terms that are important when the particles have density of the same order of the fluid, which we denote 'light particles' throughout the paper.

Most of the research on stability of particle laden flows discusses heavy particles. Saffman in 1962 [12] showed theoretically that adding dust to a gas might stabilize the flow. Michael in 1964 [13] confirmed the results by Saffman by showing neutral stability curves for several particle sizes. His findings show that an optimal particle relaxation time exists for maximum stabilization. Both Saffman and Michael considered a plane parallel Poiseuille flow in which the base flow particle velocity equals the base flow of the fluid. Both the fluid and the particles are modeled in a Eulerian framework. In addition, particles are considered spherical and homogeneously distributed.

Rudyak *et. al.* [14] and Asmolov and Manuilovic [15] extended the linear stability analysis in channel and boundary layer flow by improving the numerical accuracy using a different technique based on integration in the complex plane. Modal analysis is also considered in Klinkenberg *et al.* [10]. These authors show that stabilization due to heavy particles arises when the ratio of particle relaxation time and the period of the instability, the stability Stokes number, is of order one.

Non-modal analysis is a relatively new, but an important tool to predict instabilities. Nowadays it is understood that a perturbation in a shear flow can experience significant transient energy growth [16–19]. This growth is responsible for the initial linear amplification of disturbances which leads to subcritical transition to turbulence. Non-modal effects can therefore explain the discrepancy observed between the critical Reynolds number for linear instability and the experimental observations of transition in wall-bounded shear flows. One needs therefore to consider also non-modal analysis to gain insight into the stability of wall-bounded flows seeded with light particles. Klinkenberg *et al.* [10] investigated non-modal growth in channel flow seeded with heavy particles and found that particles have little effect on the flow stability.

The general equations for particle-laden flows given by Maxey and Riley in 1983 [20] provide an overview of the particle-fluid interaction forces. These forces consist of the Stokes drag, the added mass, the fluid acceleration force (also known as pressure correction force), buoyancy and the Basset history term. The starting point of their analysis is the equation of motion proposed by Tchen [21] and modified by Corrsin and Lumley [22]. Besides these interaction forces, the Saffman lift force [23] may also be relevant, as discussed by several authors [24–26] and more recently by Boronin and Osiptsov [27]. In addition to these different interaction terms, the effect of finite particle volume, the volume the particles have, is investigated by Vreman [28] and Boronin [29]. In the present paper Stokes drag, added mass, fluid acceleration and Basset history force are considered, limiting the validity of our analysis to small particles.

Although the different forces between fluid and particles have been known for a long time and have been discussed for turbulent flows in several papers, e.g. Calzavarini *et.al.* [30], transitional flows with light particles have not been often investigated in literature. Relevant work on transition in particle-laden flows is presented by Matas *et. al.* [31, 32]. These authors performed experiments in a pipe flow seeded with neutrally buoyant particles. To control transition to start at $Re \approx 2100$ in a clean flow, they inserted a ring at the pipe entrance. Particles of four different sizes were injected into the flow and the Reynolds number at which transition starts, the transitional Reynolds number, investigated. All particle sizes stabilized the flow for large concentrations, i.e. the transitional Reynolds number increased. For smaller concentrations (volume fraction ≤ 0.2), large particles destabilized the flow, while the smaller particles ($d/D \leq 70$) stabilized the flow. Interestingly, in the range of small particles, the results became independent of the particle diameter.

The aim of this paper is to investigate modal and non-modal stability of particle suspensions for a wide range of density ratios. To perform our analysis, we adopt the model introduced in Ref. [20], rewritten into a Eulerian framework. While this continuous approach is likely to fail in turbulent flows due to particle clustering and singularities in the particle field, it can still be used for laminar flows and perturbation expansions,

such as in linear stability calculations [33]. Instead of modeling both fluid and particles in a Eulerian framework, the particles can also be solved by Lagrangian tracking. Meiburg *et al.* [34] investigated the behavior of heavy particles in a 2D-mixing layer using two-way coupling in a Eulerian-Lagrangian framework. They found a vorticity-based understanding of the propagation of a traveling wave.

2 Flow model and stability analysis

Few approximations exist for the coupling between fluid and solid phase depending on the particle size and volume fraction, see Elghobashi [35]. As a first step in the analysis of the stability of particle laden flows, we neglect collisions and hydrodynamic coupling and therefore use the two-way coupling model. The two-way coupling includes Stokes drag, added mass, fluid acceleration and Basset history force. We are first interested in the influence of added mass and fluid acceleration on the stability and therefore neglect buoyancy. The Basset history force accounts for the development of the boundary layer on the particles and its effect is studied in Sect. 4.

2.1 Governing equations

The governing equations are the Navier Stokes Equations with the addition of the different fluid-particle interaction terms, written in a Eulerian framework. The dimensional equation for the total particle field reads [36]:

$$\frac{du_{p_i}}{dt} = \frac{\rho_f}{\rho_p}\frac{Du_i}{Dt} - \frac{1}{2}\frac{\rho_f}{\rho_p}\left[\frac{du_{p_i}}{dt} - \frac{Du_i}{Dt}\right] + \frac{K}{m_p}(u_i - u_{p_i}), \tag{1}$$

with u_i the fluid velocity, u_{p_i} the particle velocity and $i = 1-3$. $m_p = 4/3\pi r^3 \rho_p$ is the particle mass, ρ_p and ρ_f the density of the particle and the fluid, $m_f = 4/3\pi r^3 \rho_f$ the fluid mass ideally contained by the volume of one particle, and $K = 6\pi r\mu$ the Stokes drag term with μ the fluid kinematic viscosity and r the particle radius. The notation D/Dt is used for the total derivative following a fluid element, while d/dt is used for the total derivative following a moving particle. The terms on the right-hand side of Eq. (1) are the fluid acceleration, added mass and Stokes drag respectively. The particle relaxation time is defined as $\tau = \frac{m_p}{K}$. In the particle momentum equation the particle-particle interaction has been neglected. Although such interactions are important when the volume fraction is large, we chose to neglect these and restrict the maximum particle volume fraction, as discussed in Sect. 2.2. To account for particle-particle interactions, a viscosity and pressure could be defined in the particle momentum equation. More information on the modeling of particle-particle interactions in a two-fluid model can be found in [37].

The counterpart is the momentum equation for the fluid

$$\rho_f \frac{Du_i}{Dt} = -m_f N \frac{Du_i}{Dt} + \frac{1}{2} m_f N\left[\frac{du_{p_i}}{dt} - \frac{Du_i}{Dt}\right] - KN(u_i - u_{p_i}) - \frac{\partial p}{\partial x_i} + \mu\frac{\partial^2 u_i}{\partial x_j^2}, \tag{2}$$

with $i = 1-3$, N the number of particles per unit volume.

When every term is made non-dimensional with the channel half-width L, centerline velocity U, we obtain the following non-dimensional particle and fluid momentum equations:

$$\frac{du_{p_i}}{dt} = \xi\frac{Du_i}{Dt} - \frac{1}{2}\xi\left[\frac{du_{p_i}}{dt} - \frac{Du_i}{Dt}\right] + \frac{1}{SR}(u_i - u_{p_i}), \tag{3}$$

$$(1-\Phi)\frac{Du_i}{Dt} = -\frac{\partial p}{\partial x_i} + \frac{1}{R}\frac{\partial^2 u_i}{\partial x_j^2} - f\xi\frac{Du_i}{Dt} - \frac{1}{2}f\xi\left[\frac{Du_i}{Dt} - \frac{du_{p_i}}{dt}\right] + \frac{f}{SR}(u_{p_i} - u_i), \tag{4}$$

with $i = 1-3$. The different dimensionless numbers are defined in Table 1. These are the mass concentration f, the mass of particles for unit volume of the suspension over the density of the fluid, the density ratio ξ and the volume concentration Φ, the volume occupied by the particles over the total volume of the suspension. The particle relaxation time τ is either non-dimensionalized with the viscous time scale of the flow (S) or the advective time scale (SR). Note that the fluid equation (2) is defined using the total volume. To

Table 1 Definition of the non-dimensional numbers

f	$\frac{m_p N}{\rho_f}$	Mass concentration
ξ	$\frac{\rho_f}{\rho_p}$	Density ratio
Φ	$f\xi$	Volume concentration
R	$\frac{\rho_f U L}{\mu}$	Reynolds number
S	$\frac{\nu\tau}{L^2}(=\frac{2}{9}\frac{r^2}{L^2}\frac{\rho_p}{\rho_f})$	Viscous Relaxation time
SR	$\frac{U\tau}{L}$	Stokes number

account for the particle volume we have to multiply the density with $(1-\Phi)$.

The dimensionless numbers in Table 1 are not independent of each other and only 4 of them are strictly necessary. The volume fraction, density ratio and Mass fraction are coupled through $\Phi = f\xi$. Also the Reynolds number and dimensionless relaxation time S can be coupled into the Stokes number SR. Although not all the non-dimensional numbers reported in the table are independent, we define all of them to clarify how they change when varying some of the basic features of the flow or of the particles. For instance, we may wish to investigate the importance of either the density ratio, the size of the particles or the volume fraction independently and thus change the different non-dimensional number in a less obvious way. The size of the particles, as example, appears in several of these dimensionless numbers.

In addition to the momentum equations, conservation of mass is necessary to close the system; for particles and fluid these read

$$\frac{\partial f}{\partial t} = -\frac{\partial}{\partial x_i}(f u_{p_i}) \tag{5}$$

$$\frac{\partial u_i}{\partial x_i} = 0, \tag{6}$$

with $i = 1-3$. To study linear stability, a small perturbation (u') to a base flow (U) is introduced, where the base flow is considered to be the parallel Poiseuille flow, $U = U(y) = 1-y^2$, with $y \in [-1, 1]$. The particle base flow is equal to the fluid base flow, independent of the number of particles. Substituting $u_i = U + u_i'$, $u_{p_i} = U + u_{p_i}'$, $p = P + p'$ and $f = f' + f_0$ in (4)–(6), linearized stability equations are derived in a standard way [19]. f_0 is considered a homogeneous mass fraction of particles and f' is a small deviation from that homogeneous condition. The linearized equations read (primes are omitted except for f' and $f = f_0$):

$$\begin{aligned}(1-\Phi)\frac{\partial u_i}{\partial t} = &-\frac{\partial p}{\partial x_i} - (1-\Phi)U_j\frac{\partial u_i}{\partial x_j} \\ &- (1-\Phi)u_j\frac{\partial U_i}{\partial x_j} + \frac{1}{R}\frac{\partial^2 u_i}{\partial x_j^2} \\ &+ \frac{f}{SR}(u_{p_i} - u_i) + f\cdot(AM + FA)\end{aligned} \tag{7}$$

$$\begin{aligned}\frac{\partial u_{p_i}}{\partial t} = &-U_j\frac{\partial u_{p_i}}{\partial x_j} - u_{p_j}\frac{\partial U_i}{\partial x_j} + \frac{1}{SR}(u_i - u_{p_i}) \\ &+ AM + FA\end{aligned} \tag{8}$$

$$\frac{\partial f'}{\partial t} = -\nabla\cdot\left(f'U + f u_{p_i}\right) \tag{9}$$

$$\frac{\partial u_i}{\partial x_i} = 0. \tag{10}$$

With $i = 1-3$, AM and FA the Added Mass and Fluid Acceleration, with subscripts $_f$ and $_p$, denoting fluid and particle respectively:

$$\begin{aligned}AM = -\frac{1}{2}\xi\Bigg(&\frac{\partial}{\partial t}(u_i - u_{p_i}) + U_j\frac{\partial}{\partial x_j}(u_i - u_{p_i}) \\ &+ (u_i - u_{p_i})\frac{\partial U_i}{\partial x_j}\Bigg),\end{aligned} \tag{11}$$

$$FA = -\xi\left(\frac{\partial u_i}{\partial t} + U_j\frac{\partial u_i}{\partial x_j} + u_j\frac{\partial U_i}{\partial x_j}\right), \tag{12}$$

with $i = 1-3$. For the configuration considered, the equation for the particle mass fraction f' (9) is decoupled from the rest of the system. As a consequence, Squires theorem can be extended to this case and a complex Orr-Sommerfeld equation can be derived. Reference [29] This has been done in Ref [12, 13] for heavy particles, but the approach can be extended to incorporate the added mass and fluid acceleration. However, we are here interested in the non-modal stability of the full three-dimensional problem and therefore consider the corresponding initial value problem. The equations for the fluid velocities are rewritten into wall-normal velocity v and wall-normal vorticity $\eta = \frac{\partial u}{\partial z} - \frac{\partial w}{\partial x}$, analogous to the standard Orr-Sommerfeld-Squire system used for parallel single phase flows. This is done by eliminating the pressure from Eq. (7) and by solving for $\frac{\partial u}{\partial z} - \frac{\partial w}{\partial x}$. The corresponding total system of particle and fluid equations then

reads

$$\left(1+\frac{1}{2}f\xi\right)\frac{\partial}{\partial t}\nabla^2 v-\frac{1}{2}f\xi\frac{\partial}{\partial t}Q$$
$$=\left\{-\left(1+\frac{1}{2}f\xi\right)\left[U\frac{\partial}{\partial x}\nabla^2-U''\frac{\partial}{\partial x}\right]-\frac{f}{SR}\nabla^2+\frac{1}{R}\nabla^4\right\}v$$
$$+\frac{1}{2}f\xi\left[-U''\frac{\partial v_p}{\partial x}-U'\frac{\partial}{\partial x}\nabla\cdot\vec{u}_p+U\frac{\partial}{\partial x}Q\right]+\frac{f}{SR}Q \tag{13}$$

$$\left(1+\frac{1}{2}f\xi\right)\frac{\partial\eta}{\partial t}-\frac{1}{2}f\xi\frac{\partial}{\partial t}\left(\frac{\partial u_p}{\partial z}-\frac{\partial w_p}{\partial x}\right)$$
$$=-\left(1+\frac{1}{2}f\xi\right)\left(U\frac{\partial\eta}{\partial x}+U'\frac{\partial v}{\partial z}\right)+\frac{1}{2}f\xi\left(U'\frac{\partial v_p}{\partial z}+U\frac{\partial}{\partial x}\left(\frac{\partial u_p}{\partial z}-\frac{\partial w_p}{\partial x}\right)\right)+\frac{f}{SR}\left(\frac{\partial u_p}{\partial z}-\frac{\partial w_p}{\partial x}-\eta\right)+\frac{1}{R}\nabla^2\eta \tag{14}$$

with

$$Q=\frac{\partial^2 v_p}{\partial x^2}+\frac{\partial^2 v_p}{\partial z^2}-\frac{\partial^2 u_p}{\partial x\partial y}-\frac{\partial^2 w_p}{\partial z\partial y}. \tag{15}$$

The boundary conditions of this system are $v=\eta=u_p=v_p=w_p=0$ at top and bottom walls. In the Appendix, the matrix representation of this system can be found which is used to solve the eigenvalue problem.

Note finally that the Reynolds number of the flow is defined as $R=\frac{\rho_f UL}{\mu}$. While this can be seen as a Reynolds number for the fluid alone, a modified Reynolds number can be defined for the total system as:

$$R_m=\frac{(1+f-\Phi)\rho_f UL}{\mu},$$

thus based on the total density. This modified Reynolds number R_m is used in the modal analysis, whereas the Reynolds number R is used when presenting results from non-modal stability.

2.2 Model limitations

The model used here implies some limitations on the plausible values of the particle parameters. The parameters to be considered are the volume fraction, the density ratio and the size of the particles. When two-way coupling is used, the volume fraction should not be too large, because collisions and hydrodynamic coupling are not modelled. This limitation is best illustrated using the average particle spacing: $\frac{l}{D}\sim(\frac{\pi}{6\Phi})^{1/3}$, with l the average particle spacing and D the diameter of the particle. For a volume fraction of $\Phi=0.01$, the average particle spacing $\frac{l}{D}\sim 3.74$. Although the physical particle spacing below which particle-particle interactions play a role is not clearly defined, in this paper we limit the volume fraction to $\Phi=0.01$.

The limits on the density ratio are given by the fact that particles cannot be too light since we neglect surface tension and deformability. Here we will therefore limit the results to the case $\xi\leq 2$. In addition buoyancy effects become relevant when $\xi\neq 1$. These forces will be however neglected in this study to simplify the problem and to be able to focus on the effect of the other interaction forces (added mass and acceleration). Buoyancy effects, and related phenomena like sedimentation, are left as future work. Note also that neutrally buoyant small particles have no effect on the flow dynamics in the limit considered here; neutrally buoyant particles however have significant effects on the flow for volume fractions larger than 0.01 [31, 38].

The third limiting parameter is the size of the particles, r/L, where r is the radius of the particle and L the channel half-height. For large particles finite-size effects needs to be included, as in the so-called Faxen correction. In addition, we need sufficiently many particles to assume a continuous homogeneous particle distribution. Given a specific volume fraction, the size and the number of particles are coupled: the smaller the particle, the more particles are needed to obtain this volume fraction. This dependence is shown in Fig. 1 where the particle volume is given as a function of the number of particles for different particle sizes. Two limits are also shown, $\Phi=0.01$ and $N=1000$: with a volume fraction $\Phi=0.01$ and a minimum number of $N=1000$ particles, the maximum size of the particles becomes $r/L=0.0134$. This is therefore the order of magnitude for the maximum size allowed by the model adopted for this work.

Although these are the physical limitations of our model, in some of the following figures we may also show data outside this range to emphasize the effect of the solid dispersed phase on the stability of channel flow.

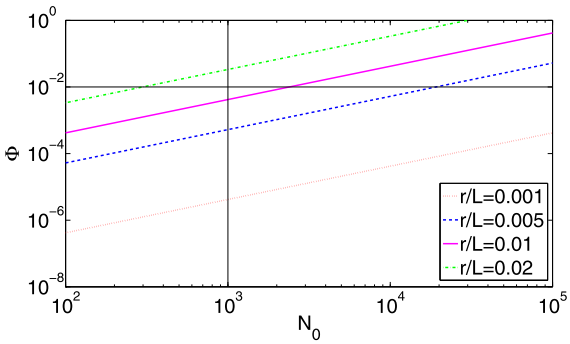

Fig. 1 Particle volume versus number of particles, for different particle sizes. N_0 is the number of particles per unit volume. The two limits ($\Phi = 0.01$ and $N = 1000$) are shown as thin *black lines*. The intersection of these *lines* coincides with a particle size $r/L = 0.0134$. Larger particles fall outside the limits of the approximations used in this paper

2.3 Modal stability analysis

To study linear stability, we assume wave-like perturbations of the following form:

$$q = \hat{q}(y)e^{i(\alpha x+\beta z-\omega t)},$$

with $q = (v, \eta, u_p, v_p, w_p)^T$. In the expression above, α and β define the streamwise and spanwise wavenumber of the perturbation respectively and ω is a complex frequency. The temporal problem is considered here: when $\Im(\omega) > 0$, the perturbation will grow exponentially in time. Conversely, when all $\Im(\omega) < 0$, all disturbances decay asymptotically, i.e. the flow is stable. The point where $\omega_i = 0$, is called neutrally stable. When computing ω_i in a range of wavenumbers α and Reynolds numbers, a neutral stability curve can be obtained. This curve defines the range where exponentially unstable waves can be found. As mentioned earlier, the neutral stability curve can be computed assuming two-dimensional perturbations, since a modified version of Squire's theorem holds for particle laden flows [12, 29].

2.4 Non-modal stability analysis

Transient disturbance energy growth may appear when the eigenvectors of the system are non-normal. This is also the case in systems that are asymptotically stable. To investigate transient growth, non-modal analysis is necessary. Non-modal analysis determines the largest possible growth of a perturbation in a finite time interval, also called optimal growth. The initial disturbance yielding optimal growth is called an optimal initial condition.

The discretized governing linear equations can be written in compact form as:

$$\frac{\partial q}{\partial t} = Lq. \tag{16}$$

The largest possible growth at time t is the norm of the evolution operator, or propagator, $\mathcal{T} = \exp(tL)$. This propagator takes any initial condition from $t = 0$ to a specified final time t. The maximum amplification is defined as:

$$\max_{q_0} \frac{\|q\|}{\|q_0\|} = \max_{q_0} \frac{\|\exp(tL)q_0\|}{\|q_0\|} = \|\exp(tL)\| \equiv G(t). \tag{17}$$

The norm used should be relevant to our problem. Therefore we use the kinetic energy of the full system defined as the kinetic energy of the fluid and of the particles together:

$$E_{kin} = \frac{1}{2}\left(m_f u_i^2 + m_p u_{p_i}^2\right), \tag{18}$$

with m_f and m_p the mass of the fluid and the particles respectively.

A matrix M can be constructed to compute the kinetic energy. This matrix M is applied directly to the vector $q = [v, \eta, u_p, v_p, w_p]^T$ to give the kinetic energy integrated over the volume V

$$E(t) = \frac{1}{2}\int_\Omega q^H M q dV. \tag{19}$$

With this definition the optimal growth is defined as the 2-norm of the modified propagator

$$\max_{q_0} \frac{\|q\|_E}{\|q_0\|_E} = \max_{q_0} \frac{\|Fq\|_2}{\|Fq_0\|_2} = \max_{q_0} \frac{\|F\exp(tL)F^{-1}Fq_0\|_2}{\|Fq_0\|_2} = \|F\exp(tL)F^{-1}\|_2 \equiv G(t) \tag{20}$$

where F is the Cholesky factorization of $M = FF^H$.

As in our previous study, we are not only interested in optimizing the total energy of the system, but also

wish to investigate the optimal growth when perturbing only the fluid or particle velocity. In this case, we do not consider the total kinetic energy of the system, but only a part of it, depending on the initial condition and final state chosen. This separation can be achieved by including either fluid or particle energy when computing the optimal growth. [10] The optimization can be written as

$$\begin{aligned} G(t) &= \frac{\|q_{out}(t)\|_{E_{out}}}{\|q_{in}(0)\|_{E_{in}}} \\ &= \frac{\|\mathcal{T} q_{in}(0)\|_{E_{out}}}{\|q_{in}(0)\|_{E_{in}}} \\ &= \frac{\|F_{out}\mathcal{T} q_{in}(0)\|_2}{\|F_{in} q_{in}(0)\|_2} \\ &= \frac{\|F_{out}\mathcal{T} F_{in}^{-1} F_{in} q_{in}(0)\|_2}{\|F_{in} q_{in}(0)\|_2} \\ &= \|F_{out}\mathcal{T} F_{in}^{-1}\|_2 \\ &= \|F_{out} C \exp(tL) B F_{in}^{-1}\|_2 \end{aligned} \tag{21}$$

Here, the propagator $\mathcal{T} = C\exp(tL)B$ is rewritten to include the input and output matrices. The input is $q_{in} = Bq$, while $q_{out} = Cq$ is the output we are interested in. The energy norm must be separated likewise, $M_{in} = F_{in}F_{in}^H$ is applied to q_{in} to measure the input energy while $M_{out} = F_{out}F_{out}^H$ gives the output energy. In the classic non-modal analysis discussed, $F_{in} = F_{out}$ and $C = B = I$.

2.5 Numerical method

The discretization in y-direction of the equations is done using the Chebyshev collocation method. [39]. Most computations are performed using $n_y = 37$, with n_y the number of collocation points. Several cases have also been computed with $n_y = 67$ to validate the accuracy of the results.

For the transient growth computation, we made use of the following energy matrix M:

$$M = \begin{pmatrix} (-\frac{D^2}{k^2}+1)I_w & 0 & 0 & 0 & 0 \\ 0 & \frac{1}{k^2}I_w & 0 & 0 & 0 \\ 0 & 0 & fI_w & 0 & 0 \\ 0 & 0 & 0 & fI_w & 0 \\ 0 & 0 & 0 & 0 & fI_w \end{pmatrix}. \tag{22}$$

In the expression above, I_w is the diagonal matrix performing spectral integration in y direction. This matrix can be easily factorized using a singular value decomposition (SVD): $M = U\Sigma U^H = FF^H$.

3 Results

3.1 Modal analysis

The results for modal stability analysis are given in Fig. 2, where we display the critical total Reynolds number versus the dimensionless, viscous particle relaxation time S in (a). Particles heavier than the fluid increase the critical Reynolds number. The largest stabilization is found when considering heavy particles and the only relevant interaction term is the Stokes drag. Lighter particles, but still heavier than the fluid, also increase the critical Reynolds number. Particles lighter than the fluid ($\xi > 1$ and still rigid in our model) behave oppositely to heavy particles and decrease the critical Reynolds number. The results in

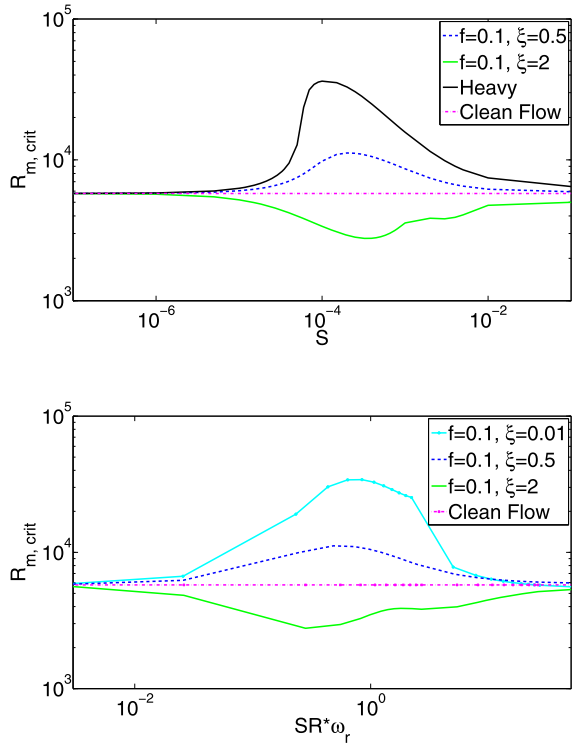

Fig. 2 Critical Reynolds number as a function of dimensionless relaxation time S and of stability Stokes number $SR\omega_r$ for light particles using both added mass and fluid acceleration: ξ=[0.5, 2], $f = 0.1$. The results for heavy particles with large density ratio (Stokes drag only) is also given as reference

Fig. 2(b) show that the largest critical Reynolds number is found when the stability Stokes number $SR\omega_r \approx 1$, where the stability Stokes number is defined as the Stokes number times the period of the disturbance wave. The stability Stokes number therefore, is the ratio between the dimensionless, advective particle relaxation time and the timescale of the disturbance.

To gain further understanding on the modal stability of particle-laden flows, we examine the critical Reynolds number as a function of density ratio in Fig. 3(a). The mass fraction is prescribed together with the dimensionless particle size and we can clearly distinguish the effects of both parameters: (i) The mass fraction influences the values of the maximum critical Reynolds number. (ii) The particle size influences the density ratio at which the maximum Reynolds number is reached. When the particle size increases, the maximum critical Reynolds number is shifted to lighter particles. The latter finding can be explained by the definition of $S = \frac{2}{9}\frac{r^2}{L^2}\frac{1}{\xi}$, which is a function of the particle size and density ratio. The largest stabilization is indeed found for stability Stokes number of order one, as shown previously.

In Fig. 3(b) we display the critical Reynolds number versus the dimensionless particle size, r/L. If we consider small particles, the critical Reynolds number is not affected by the inclusion of particles. When particle size increases, we see the increased critical Reynolds number for values in the range $r/L = 0.001 < r/L < 0.01$. The size at which the critical Reynolds number is maximum is related to the density ratio: the particle relaxation time S depends linearly on $\xi = \Phi/f$. Note that the data for heavy particles are obtained using Stokes drag only. Fixing the same volume and mass fraction as for light particles $\xi = \Phi/f$, the size is defined by $r/L = \sqrt{9/2S\xi}$ as a function of dimensionless relaxation time S. This definition also explains why small particles hardly have an effect. For small r/L, also S is small and we have seen before (Fig. 2) that at small dimensionless relaxation times particles do not affect modal stability.

The effect of added mass and fluid acceleration on the critical Reynolds is examined in Fig. 4. The results in the figure are obtained using Stokes drag and either added mass or fluid acceleration. The added mass term shows the same trend as obtained with Stokes drag only: the critical Reynolds number increases, see Fig. 4(a). When the particles become heavier, the stability curve computed with added mass

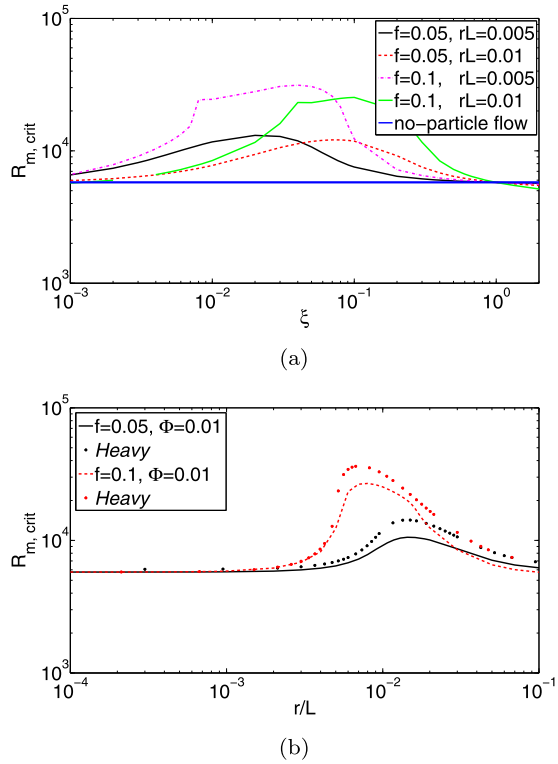

Fig. 3 Critical Reynolds number as a function of the density ratio ξ for two mass fractions and particle sizes (**a**) and the critical Reynolds number as a function of particle size r/L for two mass fractions and $\Phi = 0.01$ (**b**). In (**b**) we report also the results for heavy particles with large density ratio when only Stokes drag is used

overlaps with that for heavy particles. The figure indicates that the lighter the particle, the lower the critical Reynolds number when considering only added mass. Fig. 4(b) shows the results obtained considering fluid acceleration and Stokes drag. For $\xi = 0.1$ the critical Reynolds number is very close to that for heavy particles. For larger values of ξ, the critical Reynolds number decreases. Particles lighter than the fluid destabilize the flow and reduce the critical Reynolds number, as shown for $\xi = 2$.

The results obtained including the fluid acceleration force are similar to those shown before when all terms are used. Thus, the fluid acceleration is the dominant force in the system. The fluid acceleration force is proportional to $\frac{Du_i}{Dt}$ whereas the Added Mass to $(\frac{Du_i}{Dt} - \frac{du_{p_i}}{dt})$. The fact that the fluid acceleration force is the most dominant of the two indicates that $\frac{Du_i}{Dt}$ and $\frac{du_{p_i}}{dt}$ tend to be of the same order for light particles.

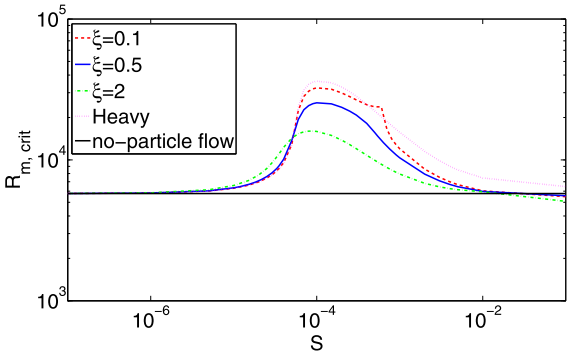

(a) Added mass

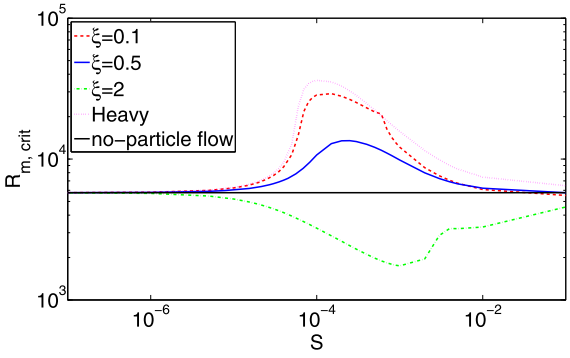

(b) Fluid acceleration

Fig. 4 Critical Reynolds number vs. relaxation time S for particles of density ratio ξ=[0.1, 0.5, 2] and mass fraction $f = 0.1$. As reference, we display the results for clean flow and heavy particles (Stokes drag only). In (**a**) Stokes drag and added mass, in (**b**) Stokes drag and fluid acceleration are used as interaction terms

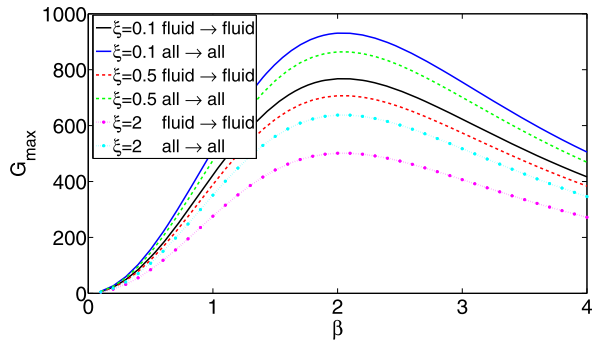

(a)

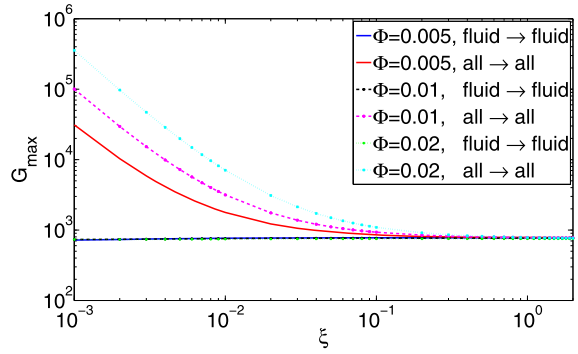

(b)

Fig. 5 (**a**) Optimal growth (G_{max}) as a function of spanwise wave-number β at $S = 5 \times 10^{-5}$, $f = 0.1$ and $R = 2000$. The cases fluid → fluid and all → all are presented for $\xi = [0.1, 0.5, 2]$. (**b**) Optimal growth as a function of ξ using $\beta = 2$ at $S = 5 \times 10^{-5}$, $r/L = 0.01$ and $R = 2000$ for $\Phi = [0.005, 0.01, 0.02]$

3.2 Non-modal analysis

Results of the non-modal analysis are presented in Fig. 5. The only cases presented are those denoted fluid → fluid and all → all. The first case investigates the transient growth of the fluid energy when the initial condition consists of fluid perturbation only; the optimal growth of the fluid disturbance velocity is studied. The particles are in the system and can gain energy, but this is not apparent. In the case all → all, the total energy of the two-phase system is investigated and particles may have some initial disturbance velocity. In Fig. 5(a), we display the optimal growth as a function of spanwise wave-number β, the streamwise wave-number α is set to zero. The data represent the maximum over the final optimization time. The computations are performed for 2D waves as well; since the transient growth of these streamwise waves is two orders smaller than for spanwise waves these results will be presented later. The density ratios under consideration are those used also in the modal analysis, $\xi = [0.1,\ 0.5,\ 2]$. For all → all we see an increase of the optimal growth by a factor $(1 + f - \Phi)^2$. The increase can be explained by using the modified Reynolds number R_m. The optimal growth is proportional to R^2, and with the modified Reynolds number defined previously, we see that the optimal growth therefore should increase by $(1 + f - \Phi)^2$. For fluid → fluid we find transient growth smaller than for a clean flow. This is caused by the fact that there is less fluid per unit volume, $(1 - \Phi)$, part of the fluid volume is taken by particles. Thus, a modified Reynolds number based on the fluid density alone is smaller and therefore the disturbance growth is also smaller. If we include the density variations in the system in a modified Reynolds number, the results with all extra forces included are

similar to those for heavy particles, namely there is no significant effect of particles on the streak transient growth. In the second figure, Fig. 5(b), the particle size and total volume is set, while the density ratio is changed along the horizontal axis. Note that the mass fraction is a function of density ratio and volume fraction, $f = \Phi/\xi$. For small values of ξ, the mass fraction is large and thus the growth for the case all $\rightarrow$ all is larger. This effect is the same as in Fig. 5(a): the optimal growth increases by $(1 + f - \Phi)^2$. The case fluid $\rightarrow$ fluid hardly changes: as the volume fraction is fixed and the growth scales as $(1 - \Phi)$, particles have negligible effect on the amplification of the fluid kinetic energy.

The effect of the added mass and fluid acceleration on the streak transient growth is further investigated for several values of S using the spanwise wavenumber $\beta = 2$, where the optimal growth is at the maximum. These results can be found in Fig. 6. First we note in 6(a) that for the cases all $\rightarrow$ all the maximum possible amplification starts to diverge for $S > 1 \times 10^{-2}$; this is due to the decoupling of particle and fluid behavior at high Stokes number, discussed for heavy particles in [10]. This indicates that the two additional forcing terms present in the case of lighter particles do not influence the growth at large values of S and therefore the results are consistent with those for heavy particles.

As noted above, the energy amplification is larger when considering both fluid and particle energy (all $\rightarrow$ all) than for fluid alone (fluid $\rightarrow$ fluid). Figure 6(a) shows that at fixed mass fraction, the energy growth for the fluid $\rightarrow$ fluid case is almost equal to that for clean fluid and independent of the particle density ratio. Only at very large values of S the optimal growth deviates a few percent in the presence of particles. Figure 6(b) confirms that at fixed volume fraction and particle size, the maximum growth for all $\rightarrow$ all goes as $(1 + f - \Phi)^2$. This could be seen also by plotting $G/(1 + f - \Phi)^2$ instead of G. Note that in the figure the largest values of f occur at large S.

To investigate the structures of the disturbances, we display the optimal initial condition and response in Fig. 7 for the case fluid $\rightarrow$ fluid, $S = 1 \times 10^{-3}$. The initial condition for the fluid consists of vortices, which can be seen in (a). The particle disturbance velocities are all zero. This results in streaks at the final time, where the streamwise disturbance velocity u is larger than the spanwise and wall-normal velocities

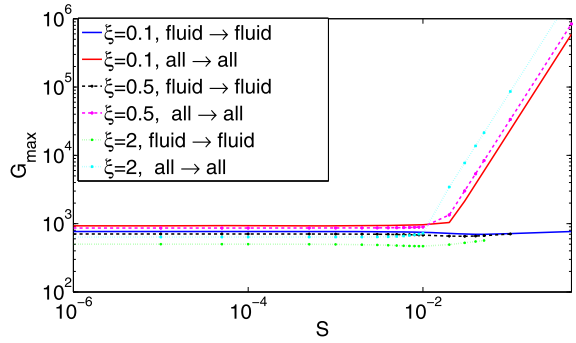

(a) f and ξ

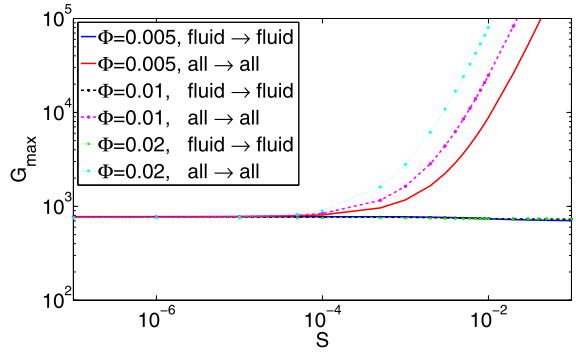

(b) r/L and Φ

Fig. 6 Optimal growth (G_{max}) as a function of S, using $\beta = 2$, $R = 2000$ and (**a**) $f = 0.1$, $\xi = [0.1, 0.5, 2]$ and (**b**) $\Phi = [0.005, 0.01, 0.02]$, $r/L = 0.01$. The cases fluid $\rightarrow$ fluid and all $\rightarrow$ all are presented

present. The velocity field of particles and fluid at final time are almost identical to each other and to the case of clean fluid (not shown here). Since differences in velocity induce a loss in energy, particles and fluid have similar velocity in optimal configurations; light particles do not induce any additional gain or loss in disturbance energy.

We therefore demonstrated how light particles have little effect on the non-modal stability of spanwise waves, confirming the results previously obtained for heavy particles. We now investigate streamwise and oblique disturbances. Even though these disturbances grow less than purely spanwise disturbances, they are important for transition in real configurations, e.g. when transition is initiated by localized disturbances. The effect of particles on these is therefore worth investigation. Figure 8 shows the results for perturbations with several streamwise α and spanwise wavenumbers β. When both are nonzero, the waves are oblique. The values of the maximum possible am-

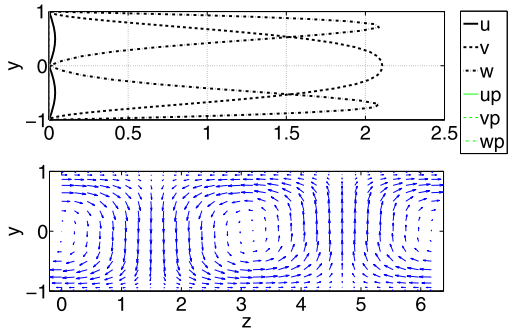

(a) Initial condition

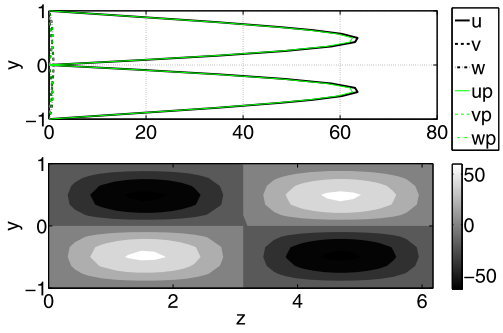

(b) Response

Fig. 7 Initial condition (**a**) and optimal response (**b**) for $S = 1 \times 10^{-3}$. Case fluid → fluid with $\xi = 2$, $\beta = 2$, $R = 2000$ and $f = 0.1$

plification for a clean fluid flow are reported in the table, whereas the curves in the figure display the relative variation with respect to the case of clean fluid. We first consider small values of the dimensional relaxation time *SR*: for two-dimensional waves ($\alpha = 1$, $\beta = 0$), particles induce a decrease in the transient growth. In our previous paper on heavy particles [10], we have shown that this reductions scales as $(1 + f)$. Streaky modes with ($\alpha = 0, \beta = 2$), conversely, display no difference between laden and unladen flow in the case of heavy particles, $\xi = 0.001$. When the density ratio increases, the growth is reduced by a factor $(1 - \Phi)^2$ for the case fluid → fluid in the figure, and as shown above in Fig. 5. Note however, that an increase of the streaks transient growth by a factor $(1 + f - \Phi)^2$ would be observed when studying the total energy in the system. For oblique waves, the results lie in between these two extremes. For slightly oblique waves ($\beta = 2, \alpha = 0.1$), we observe the lowest relative loss of energy growth. The magnitude of this loss increases for larger values of α.

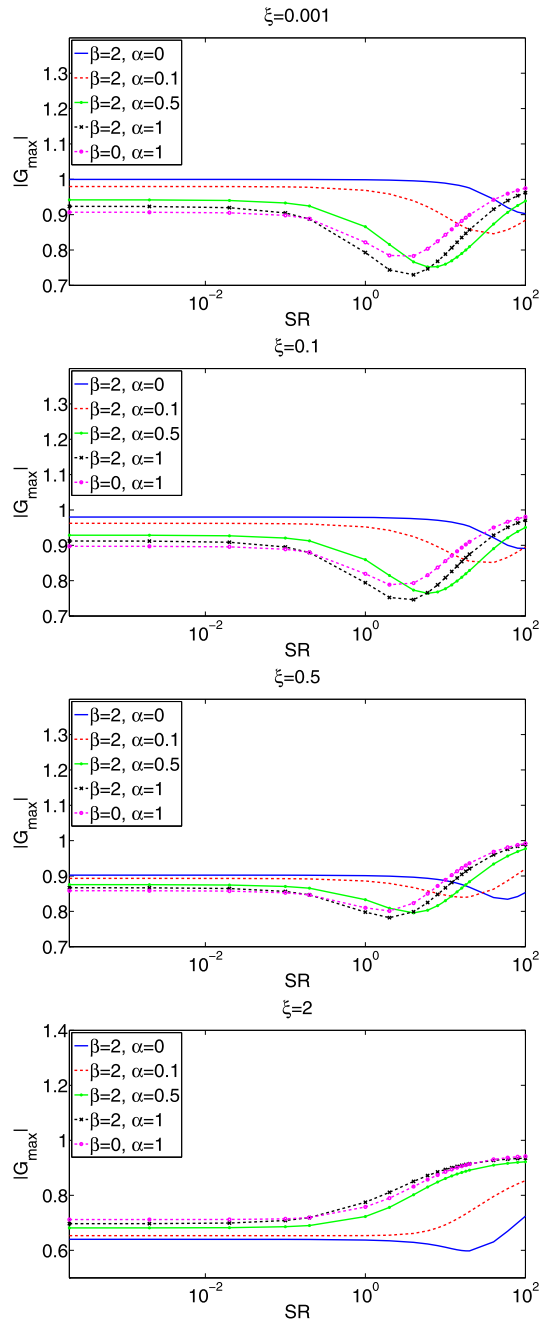

Case	Clean flow growth
$\beta = 2,\ \alpha = 0$	783.24
$\beta = 2,\ \alpha = 0.1$	664.14
$\beta = 2,\ \alpha = 0.5$	346.71
$\beta = 2,\ \alpha = 1$	193.87
$\beta = 0,\ \alpha = 1$	13.76

Fig. 8 Transient growth of oblique waves normalized with the growth rate of a clean flow as a function of *SR* for fluid → fluid and $f = 0.1$ for $\xi = [0.001,\ 0.1,\ 0.5,\ 2]$. The amplification values for a single phase fluid are reported in the table

We now consider the flow behavior at intermediate values of the Stokes number, cf. Fig. 8. A clear decrease of the transient energy growth relative to the case of single phase fluid is apparent for a range of particle relaxation times. This occurs at lower SR for two-dimensional disturbances and at larger values of SR for disturbances approaching spanwise streaky waves. This stabilization is observed for values of the stability Stokes number, defined by the ratio between the particle relaxation time and the final time giving the largest amplification, of order one. Therefore, the reduction of the amplitude of oblique disturbances is observed at lower Stokes number for modes with $\beta = 0$ for which the transient growth is faster, and at higher Stokes number for modes with $\alpha = 0$ for which the transient growth is a slower process. This stabilization is the counterpart of the increase of critical Reynolds number shown by the modal analysis. Note however, as discussed before, that the values of the Stokes number necessary to observe this stabilization can be related to parameters outside the range of validity of our model, especially for large S and therefore waves with $\beta \approx 0$. Finally, When further increasing the particle relaxation time, we observe an increase of the transient growth (values larger than 1 in the figure). Again, we note that this is however happening for particle size too large for our model to be valid.

4 Basset history force

In this section we include the Basset history term in the set of equations. First we show how this term is implemented and in the second part we discuss results for both heavy and light particles.

4.1 Numerical implementation

The Basset history term has not been considered previously for linear stability computations. The history term is different from the terms discussed so far as it appears as a convolution integral, where the total history of the fluid and particle flow has to be known. For Direct Numerical Simulations this is expensive and therefore only the recent history is usually considered. Sometimes a model to account for large times is used [40]. For stability analysis, the integral is also difficult to deal with and is therefore rewritten so that it can be implemented in a linear system.

The Basset history term is expressed as a convolution:

$$\bar{q}_i(t) = \frac{1}{Sb} \cdot \int_{-\infty}^{t} d\tau \frac{d/d\tau\{u_{p_i} - u_i\}}{[t-\tau]^{1/2}} = \frac{1}{Sb} \cdot \int_{-\infty}^{t} F(t-\tau) q(\tau) d\tau, \tag{23}$$

with $i = 1-3$ and where we approximate $\int_{-\infty}^{t} F(t-\tau)d\tau$ by an exponential; having an exponential filter

$$\bar{q}_i(t) = \int_{-\infty}^{t} C \exp\left(-\frac{t-\tau}{\Delta}\right) q(\tau) d\tau, \tag{24}$$

we can use the differential form:

$$\frac{d\bar{q}_i(t)}{dt} = Cq - \frac{\bar{q}}{\Delta}. \tag{25}$$

In this way, we are able to solve an eigenvalue problem similar to that without Basset history term, only extended with the three extra equations for $\bar{q}_i$, formally similar to Eq. (25). The matrix representation of this system is given in the Appendix. Sb is a new dimensionless number, similar to the Stokes number SR: $Sb = SR\frac{L\pi^{1/2}}{rR^{1/2}}$.

Next, we need to approximate the square root dependence of the Basset term with an exponential. Figure 9 shows the difficulty with the approximation: either the exponential is more accurate for small times, or for larger times. Several combinations of C and Δ are tested to investigate whether any combination changes the critical Reynolds number or the transient energy growth in a significant way.

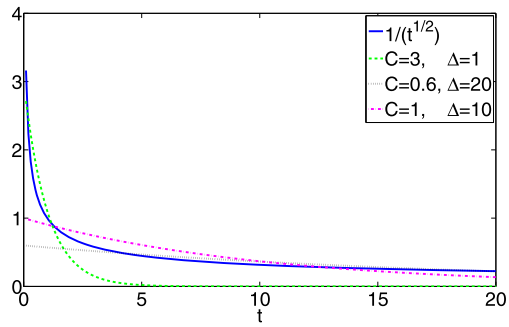

Fig. 9 The approximation of a $1/\sqrt{(t)}$ by an exponential in the form $C\exp(-t/\Delta)$

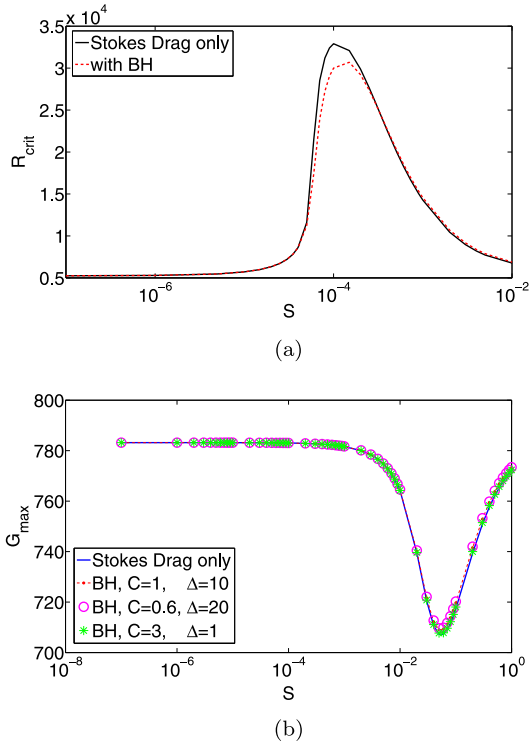

Fig. 10 Basset History with heavy particle approximation (only Stokes drag as interaction term apart from the Basset History term), $f = 0.1$ and $\xi = 0.001$. **(a)** Critical Reynolds number as a function of S. **(b)** Maximum transient growth as a function of S with $R = 2000$

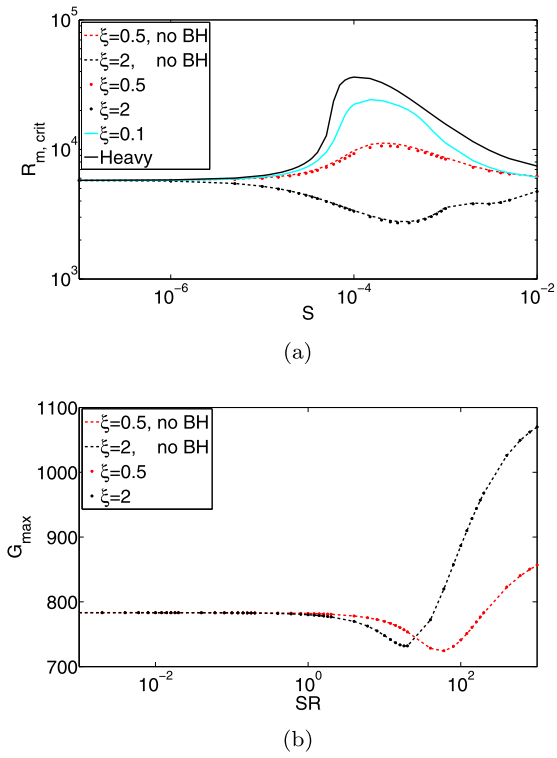

Fig. 11 Basset History with light particles with $f = 0.1$. **(a)** Critical Reynolds number as a function of S. **(b)** Maximum transient growth as a function of SR with $R = 2000$

4.2 Results

The Basset history term has not been implemented in stability of a particle laden flow before. Therefore we show first the results without added mass and fluid acceleration: the heavy particle approximation, and then include these terms. In both cases, we investigate the influence of the Basset history on both modal and non-modal stability.

For heavy particles, only a small difference is found when the history term is used, Fig. 10(a): The critical Reynolds number is decreased a few percent using $C = 3, \Delta = 1$. In non-modal analysis, Fig. 10(b), hardly anything changes for all filter parameters investigated. This could be expected due to the definition of SR and Sb. Sb is $\frac{L\pi^{1/2}}{rR^{1/2}}$ times larger than the Stokes number, thus $1/Sb$ is much smaller than $1/SR$ when $\xi = 0.001$. If we consider $SR = 1$, $R = 2000$, the size fixed at $r/L = 0.0015$, Sb is about 30 times larger than SR; thus the Basset history term is less important than Stokes drag in this regime.

When light particles are considered, the Basset history term might have an effect because the density ratio changes to $\xi \sim 1$. However, we show in Fig. 11(a) that the history term has a small effect on the critical Reynolds number. For both $\xi = 2$ and $\xi = 0.5$, the critical Reynolds number varies: The Basset history force slightly decreases the critical Reynolds number. The model used for the Basset history in this case assumes $\Delta = 1$ and $C = 3$.

Figure 11(b) shows the transient growth for light particles both with and without the Basset history term. In the figure only one set of filter parameters is used ($\Delta = 1, C = 3$), more data with different filters have been tested, but no significant difference is found.

These results imply that the Basset history affects both modal and non-modal stability for light particles in a negligible way.

5 Discussion and conclusions

We presented results for linear modal and non-modal stability of channel flow laden with particles of varying density.

Concerning modal stability, the presence of light particles changes the behavior of single-phase flow and flows seeded with heavy particles. Particles lighter than the surrounding fluid decrease the critical Reynolds number, whereas particles heavier than the fluid increase the critical Reynolds number. The decrease of the critical Reynolds number is due to the fluid acceleration term. When the fluid acceleration term is not used, but added mass and Stokes drag are, particles do increase the critical Reynolds number. The latter two interaction terms are proportional to $(\frac{Du_i}{Dt} - \frac{du_{p_i}}{dt})$ and $(u_i - u_{p_i})$ respectively, whereas the fluid acceleration is proportional to $\frac{Du_i}{Dt}$. This shows that particle and fluid velocity and their derivatives are of the same order and that therefore added mass and Stokes drag have less influence in the case of light particles. When particles are heavier, for a density ratio of $\xi = 0.1$, the results are similar to those obtained with Stokes drag alone, see Fig. 4.

The Reynolds number used in the modal-analysis is the modified Reynolds number as defined in Sect. 2.1. The increase in density due to the addition of particles is incorporated in this modified Reynolds number.

Non-modal analysis shows a more limited effect of particles. As in a clean fluid, streamwise-independent modes can undergo large non-modal growth; this is associated to the amplification of streamwise velocity streaks induced by counter-rotating streamwise vortices. The mechanisms and flow structures are equal to those observed in a single phase fluid. The interaction terms added do appear in the energy budget but do not affect the whole process; this can be explained by the long time scale associated to the streak lift-up that allows particles to follow the fluid structures. Table 2 shows the optimal growth as function of mass fraction for particle laden flows versus clean fluid for spanwise waves at small values of S. The shift by $(1 + f - \Phi)^2$ can be explained by the increased density of the total system: optimal growth is still proportional to R^2 with R based on the global suspension density. The optimal condition is that particles and fluid have equal velocities in order to minimize energy losses. Independent of which interaction forces one takes into account, the optimal growth is equal up to $S = 10^{-2}$, see Fig. 5. At larger values of S, the equations for fluid and particles decouple and the particle energy can grow infinitely in the linear model, because the only dissipative terms in the particle momentum equation stems from the forces exchanged with the fluid. Limitations in size however show that these results lie outside the validity of the present model.

Table 2 Dependence of the optimal growth with the mass fraction f for streamwise independent disturbances

Case	Dependence
all → all	$(1 + f - \Phi)^2$
fl → fl	$(1 - \Phi)^2$

When we look at streamwise-dependent disturbances, for which modal analysis reveals an increase of the critical Reynolds number, the non-modal response is smaller when compared to that in a clean fluid flow. We recall that the transient growth is at least one order of magnitude larger for spanwise-periodic streamwise-independent modes. However, oblique modes are important in the case of localized initial disturbances and at the non-linear stages of transition and thus stabilization of oblique waves can have an impact on transition as shown for the case of heavy particles. [11]

The extra interaction terms have no influence on the non-modal stability and this appears less obvious than for heavy particles. [10] The energy analysis of heavy particles shows that particle-fluid interaction always induces a loss in kinetic energy. To optimize energy, both the fluid and particles should have equal velocities, which then results in an $(1 + f - \Phi)^2$ increase of the energy gain when the particles act as passive tracers and increase the fluid density. In non-modal growth the particles act basically as passive tracer up to large values of S because transient growth is a slow process. Therefore, the stability Stokes number is small indicating that particles react to the flow faster than the time needed for the streaks to grow. These apply to both light and heavy particles.

Finally, we have used a differential form of the approximated kernel and show that the Basset history force has a negligible effect for both heavy and light particles.

Considering also the first part of this investigation [10], we see that the presence of a solid phase has no significant effect on the non-modal growth responsible

for subcritical transition in channel flows, especially in the case of elongated structures. As a next step, both particle-particle interactions and finite-size particles should be considered. For finite-size particles, we expect significant effects also for neutrally buoyant particles, see for example Matas et al. [31] and Picano et al. [41]. Also, a non-linear model should be used to investigate the effect of particles on secondary instabilities and final breakdown.

Appendix: Matrix operators for the eigenvalue problem

The equations for the particle laden flow can be written in compact form as follows:

$$M\frac{d}{dt}q = Lq, \tag{26}$$

with $q = [v,\ \eta,\ u_p,\ v_p,\ w_p]'$ without Basset History force Eqs. ((8), (13) and (14)) and

$$q = [v,\ \eta,\ u_p,\ v_p,\ w_p,\ q_1,\ q_2,\ q_3]'$$

with the Basset history force (Eqs. (8), (13) and (14) with the $\bar{q}$ defined in Eq. (25)).

The matrices M and L without the history force are defined in Eq. (27), with all the terms for velocity v given in Eqs. ((28)–(35)).

For the inclusion of the Basset history force, we do not solve any integro-differential equations. The integral associated to the Basset history term has been replaced by 3 new unknowns: $[q_1,\ q_2,\ q_3]$, see Eq. (36) where the matrices are given including the Basset history force. In here I is the identity matrix and $c = C * Sb$ with $Sb = SR\frac{L\pi^{1/2}}{rR^{1/2}}$ the dimensionless variable for the Basset history term. C and Δ are constants used to approximate the differential form of the integral in the Basset history force.

$$\underbrace{\begin{pmatrix} \mathsf{M_{vv}} & 0 & \mathsf{M_{vU}} & \mathsf{M_{vV}} & \mathsf{M_{vW}} \\ 0 & \mathsf{M_{\eta\eta}} & \mathsf{M_{\eta U}} & 0 & \mathsf{M_{\eta W}} \\ \mathsf{M_{Uv}} & \mathsf{M_{U\eta}} & \mathsf{M_{UU}} & 0 & 0 \\ \mathsf{M_{Vv}} & 0 & 0 & \mathsf{M_{VV}} & 0 \\ \mathsf{M_{Wv}} & \mathsf{M_{W\eta}} & 0 & 0 & \mathsf{M_{WW}} \end{pmatrix}}_{\mathsf{M}} \frac{d}{dt}\begin{pmatrix} \mathbf{v} \\ \eta \\ \mathbf{u_p} \\ \mathbf{v_p} \\ \mathbf{w_p} \end{pmatrix} = \underbrace{\begin{pmatrix} \mathsf{L_{vv}} & 0 & \mathsf{L_{vU}} & \mathsf{L_{vV}} & \mathsf{L_{vW}} \\ \mathsf{L_{\eta v}} & \mathsf{L_{\eta\eta}} & \mathsf{L_{\eta U}} & \mathsf{L_{\eta V}} & \mathsf{L_{\eta W}} \\ \mathsf{L_{Uv}} & \mathsf{L_{U\eta}} & \mathsf{L_{UU}} & \mathsf{L_{UV}} & 0 \\ \mathsf{L_{Vv}} & 0 & 0 & \mathsf{L_{VV}} & 0 \\ \mathsf{L_{Wv}} & \mathsf{L_{W\eta}} & 0 & 0 & \mathsf{L_{WW}} \end{pmatrix}}_{\mathsf{L}} \begin{pmatrix} \mathbf{v} \\ \eta \\ \mathbf{u_p} \\ \mathbf{v_p} \\ \mathbf{w_p} \end{pmatrix} \tag{27}$$

$$\mathsf{M_{vv}} = \left(1 + \frac{1}{2}f\xi\right)\nabla^2 \tag{28}$$

$$\mathsf{M_{vU}} = \frac{1}{2}f\xi i\alpha D \tag{29}$$

$$\mathsf{M_{vV}} = \frac{1}{2}f\xi k^2 \tag{30}$$

$$\mathsf{M_{vW}} = \frac{1}{2}f\xi i\beta D \tag{31}$$

$$\mathsf{L_{vv}} = -\left(1 + \frac{1}{2}f\xi\right)\left(i\alpha U\nabla^2 - i\alpha U''\right) - \frac{f}{SR}\nabla^2 + \frac{1}{R}\nabla^4 \tag{32}$$

$$\mathsf{L_{vU}} = -i\alpha\frac{f}{SR}D - \frac{1}{2}f\xi U i\alpha i\alpha D - \frac{1}{2}f\xi U' i\alpha i\alpha \tag{33}$$

$$\mathsf{L_{vV}} = -\frac{f}{SR}k^2 D - \frac{1}{2}f\xi U i\alpha k^2 D - \frac{1}{2}f\xi U' i\alpha D - \frac{1}{2}f\xi U'' i\alpha \tag{34}$$

$$\mathsf{L_{vW}} = -i\beta\frac{f}{SR}D - \frac{1}{2}f\xi U i\alpha i\beta D - \frac{1}{2}f\xi U' i\alpha i\beta \tag{35}$$

$$
\underbrace{\begin{pmatrix}
\mathsf{M}_{\mathbf{vv}} & 0 & \mathsf{M}_{\mathbf{v}U} & \mathsf{M}_{\mathbf{v}V} & \mathsf{M}_{\mathbf{v}W} & 0 & 0 & 0 \\
0 & \mathsf{M}_{\eta\eta} & \mathsf{M}_{\eta U} & 0 & \mathsf{M}_{\eta W} & 0 & 0 & 0 \\
\mathsf{M}_{U\mathbf{v}} & \mathsf{M}_{U\eta} & \mathsf{M}_{UU} & 0 & 0 & 0 & 0 & 0 \\
\mathsf{M}_{V\mathbf{v}} & 0 & 0 & \mathsf{M}_{VV} & 0 & 0 & 0 & 0 \\
\mathsf{M}_{W\mathbf{v}} & \mathsf{M}_{W\eta} & 0 & 0 & \mathsf{M}_{WW} & 0 & 0 & 0 \\
c\frac{i\alpha}{k^2}D & -c\frac{i\beta}{k^2}D & -cI & 0 & 0 & I & 0 & 0 \\
cI & 0 & 0 & -cI & 0 & 0 & I & 0 \\
c\frac{i\beta}{k^2}D & c\frac{i\alpha}{k^2}D & 0 & 0 & -cI & 0 & 0 & I
\end{pmatrix}}_{\mathsf{M}}
\frac{d}{dt}
\begin{pmatrix}
\mathbf{v} \\ \eta \\ \mathbf{u_p} \\ \mathbf{v_p} \\ \mathbf{w_p} \\ \mathbf{q_1} \\ \mathbf{q_2} \\ \mathbf{q_3}
\end{pmatrix}
$$

$$
= \underbrace{\begin{pmatrix}
\mathsf{L}_{\mathbf{vv}} & 0 & \mathsf{L}_{\mathbf{v}U} & \mathsf{L}_{\mathbf{v}V} & \mathsf{L}_{\mathbf{v}W} & fci\alpha D & fck^2 I & fci\beta D \\
\mathsf{L}_{\eta\mathbf{v}} & \mathsf{L}_{\eta\eta} & \mathsf{L}_{\eta U} & \mathsf{L}_{\eta V} & \mathsf{L}_{\eta W} & -fci\beta I & 0 & fci\alpha I \\
\mathsf{L}_{U\mathbf{v}} & \mathsf{L}_{U\eta} & \mathsf{L}_{UU} & \mathsf{L}_{UV} & 0 & -cI & 0 & 0 \\
\mathsf{L}_{V\mathbf{v}} & 0 & 0 & \mathsf{L}_{VV} & 0 & 0 & -cI & 0 \\
\mathsf{L}_{W\mathbf{v}} & \mathsf{L}_{W\eta} & 0 & 0 & \mathsf{L}_{WW} & 0 & 0 & -cI \\
-U' + U\frac{\alpha^2}{k^2}D & -U\frac{\alpha\beta}{k^2} & i\alpha U & 0 & 0 & -1/\Delta I & 0 & 0 \\
-i\alpha U & 0 & 0 & i\alpha U & 0 & 0 & -1/\Delta I & 0 \\
U\frac{\alpha\beta}{k^2}D & U\frac{\alpha^2}{k^2} & 0 & 0 & i\alpha U & 0 & 0 & -1/\Delta I
\end{pmatrix}}_{\mathsf{L}}
\begin{pmatrix}
\mathbf{v} \\ \eta \\ \mathbf{u_p} \\ \mathbf{v_p} \\ \mathbf{w_p} \\ \mathbf{q_1} \\ \mathbf{q_2} \\ \mathbf{q_3}
\end{pmatrix}
\tag{36}
$$

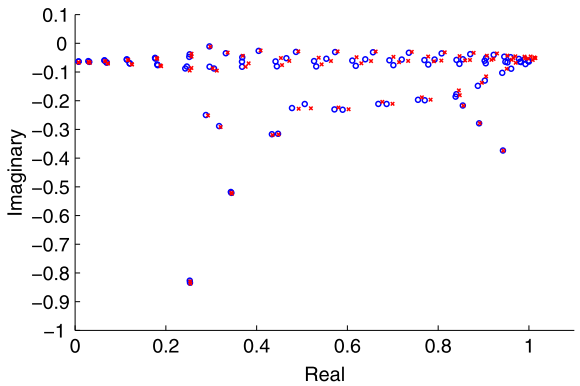

Fig. 12 Spectrum for the most unstable eigenmode for $R = 3000$, $S = 5e-3$, $\xi = 0.1$ and $f = 0.1$ with (*red cross*) and without (*blue circle*) Basset history term (Color figure online)

The eigenvalue spectra with and without Basset history term are similar to each other, as can be seen in Fig. 12 and discussed in the paper.

References

1. Toschi F, Bodenschatz E (2009) Lagrangian properties of particles in turbulence. Annu Rev Fluid Mech 41:375–404
2. Balachander S, Eaton JohnK (2010) Turbulent dispersed multiphase flow. Annu Rev Fluid Mech 42:111–133
3. Sproull WT (1961) Viscosity of Dusty Gases. Nature 190:976–978
4. Rossetti SJ, Pfeffer R (1972) Drag reduction in dilute flowing gas-solid suspensions. AIChE J 18(1):31–39
5. McCormick ME, Bhattacharyya R (1973) Drag reduction of a submersible hull by electrolysis. Naval Eng. J. 85(2):11–16
6. Jacob B, Olivieri A, Miozzi M, Campana EF, Piva R (2010) Drag reduction by microbubbles in a turbulent boundary layer. Phys Fluids 22(11):115104
7. Ferrante A, Elghobashi S (2003) On the physical mechanisms of two-way coupling in particle-laden isotropic turbulence. Phys Fluids 15:315–329
8. Xu J, Maxey MR, Karniadakis GEM (2002) Numerical simulation of turbulent drag reduction using micro-bubbles. J Fluid Mech 468:271–281
9. Zhao LH, Andersson HI, Gillissen JJJ (2010) Turbulence modulation and drag reduction by spherical particles. Phys Fluids 22:081702
10. Klinkenberg J, de Lange HC, Brandt L (2011) Modal and non-modal stability of particle-laden channel flow. Phys Fluids 23:064110
11. Klinkenberg J, Sardina G, de Lange HC, Brandt L (2013) Numerical study of laminar-turbulent transition in particle-laden channel flow. Phys Rev E 87:043011
12. Saffman PG (1962) On the stability of laminar flow of a dusty gas. J Fluid Mech 13:120–128
13. Michael DH (1964) The stability of plane Poiseuille flow of a dusty gas. J Fluid Mech 18:19–32
14. Rudyak VYa, Isakov EB, Bord EG (1997) Hydrodynamic stability of the poiseuille flow of dispersed fluid. J Aerosol Sci 82:53–66
15. Asmolov ES, Manuilovich SV (1998) Stability of a dusty-gas laminar boundary layer on a flat plate. J Fluid Mech 365:137–170

16. Ellingsen T, Palm E (1975) Stability of linear flow. Phys Fluids 18:487–488
17. Trefethen LN, Trefethen AE, Reddy SC, Driscoll TA (1993) Hydrodynamic stability without eigenvalues. Science 261:578–584
18. Reddy SC, Henningson DS (1993) Energy growth in viscous channel flows. J Fluid Mech 252:209–238
19. Schmid PJ, Henningson DS (2001) Stability and transition in shear flows. Springer, Berlin
20. Maxey MR, Riley JJ (1983) Equation of motion for a small rigid sphere in a nonuniform flow. Phys Fluids 26:883–889
21. Tchen CM (1947) Mean value and correlation problems connected with the motion of small particles suspended in a turbulent fluid. PhD thesis, Delft
22. Corrsin S, Lumley J (1956) On the equation of motion for a particle in turbulent fluid. Appl Sci Res A 6:114–116
23. Saffman PG (1992) Vortex dynamics. Cambridge Univ Press, Cambridge
24. Dandy DS, Dwyer HA (1990) A sphere in shear flow at finite Reynolds number: effect of shear on particle lift, drag, and heat transfer. J Fluid Mech 216:381–400
25. Mei R (1992) An approximate expression for the shear lift force on a spherical particle at finite Reynolds number. Int J Multiph Flow 18:145–147
26. McLaughlin JB (1991) Inertial migration of a small sphere in linear shear flows. J Fluid Mech 224:262–274
27. Boronin SA, Osiptsov AN (2008) Stability of a Disperse-Mixture Flow in a Boundary Layer. Fluid Dyn 43:66–76
28. Vreman AW (2007) Macroscopic theory of multicomponent flows: Irreversibility and well-posed equations. Physica D 225:94–111
29. Boronin SA (2008) Investigation of the stability of a plane-channel suspension flow with account for finite particle volume fraction. Fluid Dyn 43:873–884
30. Calzavarini E, Volk R, Bourgoin M, Lévêque E, Pinton J-F, Toschi F (2009) Acceleration statistics of finite-sized particles in turbulent flow: the role of Faxén forces. J Fluid Mech 630:179–189
31. Matas JP, Morris JF, Guazzelli É (2003) Transition to turubulence in particulate pipe flow. Phys Rev Lett 90:014501
32. Matas JP, Morris JF, Guazzelli É (2003) Influence of particles on the transition to turbulence in pipe flow. Philos Trans R Soc Lond A 361:911–919
33. Boffetta G, Celani A, De Lillo F, Musacchio S (2007) The Eulerian description of dilute collisionless suspension. Europhys Lett 78:14001
34. Meiburg E, Wallner E, Pagella A, Riaz A, Härtel C, Necker F (2000) Vorticity dynamics of dilute two-way-coupled particle-laden mixing layers. J Fluid Mech 421:185–227
35. Elghobashi S (1994) On predicting particle-laden turbulent flows. Appl Sci Res 52:309–329
36. Ferry J, Balachander S (2001) A fast Eulerian method for disperse two-phase flow. Int J Multiph Flow 27:1199–1226
37. van der Hoef Van MA, Annaland S, Deen NG, Kuipers JAM (2008) Numerical simulation of dense gas-solid fluidized beds: a multiscale modeling strategy. Annu Rev Fluid Mech 40(1):47–70
38. Guazzelli É, Morris JF (2011) A physical introduction to suspension dynamics. Cambridge University Press, Cambridge
39. Reddy SC, Schmid PJ, Baggett JS, Henningson DS (1998) On the stability of streamwise streaks and transition thresholds in plane channel flows. J Fluid Mech 365:269–303
40. van Hinsberg MAT, ten Thije Boonkkamp JHM, Clercx HJH (2011) An efficient, second order method for the approximation of the basset history force. J Comp Physiol 230(4):1465–1478
41. Picano F, Breugem W-P, Mitra D, Brandt L (2013) Shear thickening in non-brownian suspensions: an excluded volume effect. Phys Rev Lett 111:098302